The Study of Frequency Domain Reflectometry Technique for High Voltage Rotating Machine Winding Condition Assessment

Jialu Cheng *, Yizhou Zhang , Hao Yun , Liang Wang , Nathaniel Taylor

Posted Date: 9 August 2023

doi: 10.20944/preprints202308.0754.v1

Keywords: condition-based diagnosis; fault locating; frequency domain reflectometry (FDR); insulation degradation; rotating machines; stator winding

Article

The Study of Frequency Domain Reflectometry Technique for High Voltage Rotating Machine Winding Condition Assessment

Jialu Cheng [1,*,‡], Yizhou Zhang [2,‡], Hao Yun [2,‡], Liang Wang [2,‡] and Nathaniel Taylor [1]

[1] KTH Royal Institute of Technology, Stockholm 100 44, Sweden; jialu@kth.se
[2] China Nuclear Power Operation Technology Co., Ltd., Minzu Road 1021, Wuhan 430 073, China
* Correspondence: jialu@kth.se
‡ These authors contributed equally to this work.

Abstract: Detecting, especially locating local degradations at an incipient stage, is very important for mission-critical high voltage rotating machines. One particular challenge of the existing testing techniques is that the characteristic of a local incipient defect is not prominent due to various factors such as averaging with the healthy remainder, attenuation in signal propagation, interference, and varied operating conditions. This paper proposes and investigates the frequency domain reflectometry (FDR) technique based on scattering parameter measurement. The FDR result presents the object length, wave impedance, and reflections due to impedance discontinuity along the measured windings. Experiments were performed on two commercial coils with artificially made defects. These defects include turn-to-turn short, surface creepage, loose coils, and local overheating, which are commonly seen in practice. Two practical water pumps in the field were also selected for investigation. The study outcome shows that the FDR can identify and locate both structure and insulation degradations of both shielded and unshielded objects with good sensitivity. This makes the FDR a comprehensive tool for fault diagnosis and aging assessment.

Keywords: condition-based diagnosis; fault locating; frequency domain reflectometry (FDR); insulation degradation; rotating machines; stator winding

1. Introduction

High voltage induction motors are mission-critical assets in power plants and heavy industrial companies. Failures of these motors can lead to the revenue loss, production disruption, and even catastrophic effects on the motors and their surroundings [1,2]. Careful monitoring of excessive thermal, electrical, ambient, and mechanical (TEAM) stresses present on rotating machines over the entire service life is therefore important. It helps to reduce unexpected failure risk and replacement costs. It is of particular interest to identify the degradation at an early stage so that preventive actions can be taken.

According to the statistics [3] , stator winding problems account for approximately two-thirds of high-power motor failures. Although many techniques and commercial instruments are available for machine condition assessment [4], asset owners still face unexpected failures. The commonly used insulation diagnositic techniques are dielectric response and partial discharge (PD) testing. The dielectric response testing techniques such as Insulation resistance (IR), dissipation factor (DF), dielectric frequency response (DFR), and polarization/depolarization current (PDC) are among the most widely used techniques [5]. These methods give indications of the average winding insulation condition. But the characteristic caused by local degradation at the early stage can be dwarfed by the healthy remainder. Moreover, the threshold levels for alarming are hard to be determined because of insulation material diversity and impact of stress grading material [6,7]. Partial discharge (PD) testing is valuable for both global and local winding insulation degradation assessment [8]. Several limitations are encountered in practice: firstly, it is hard to make conclusions from a single measurement as motors

Preprints (www.preprints.org) | NOT PEER-REVIEWED | Posted: 9 August 2023 doi:10.20944/preprints202308.0754.v1

made by different manufacturers exhibit dramatically different PD activity [9]. Secondly, low-cost online PD monitoring systems can easily be disturbed by external interferences and variable speed drives [10]. Operating condition, e.g. motor slip, has a strong impact on online monitoring techniques such as vibration and motor signature current (MSC) [11]. All these limitations may lead to false indication, low sensitivity, and difficulty of fault interpretation. The sweep frequency response analysis (SFRA) method has been successful in transformer mechanical condition evaluation [12]. But it is rarely used for motors testing. Figure 1 shows an example of the SFRA testing results on a motor. The inductive property dominates most of the frequency range. Extending the upper-frequency limit further is not feasible as the measurement in the radio frequency range is fundamentally different.

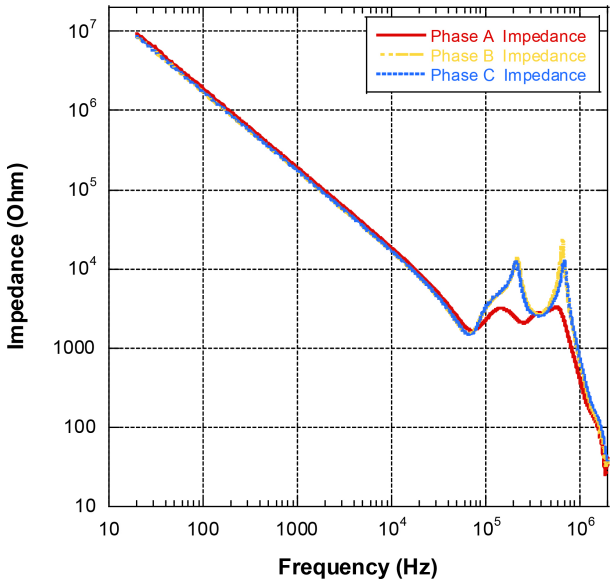

Figure 1. SFRA results of a motor.

Time Domain Reflectometry (TDR) and Frequency Domain Reflectometry (FDR) are two testing techniques in the radio frequency range. There is a long history of using TDR for cable fault pre-location but not condition diagnosis. That's because the method is relatively insensitive to subtle changes in the test circuit and subject to propagation attenuation. The use of the FDR technique for cable fault locating and aging assessment is relatively new, firstly investigated in the Halden Reactor Project around 2004 [13]. Although FDR results have a similar outlook to TDR, it has higher accuracy and sensitivity than the TDR method for subtle mechanical and insulation condition change detection [14]. This paper aims to study whether the FDR technique is suitable for stator winding condition diagnosis. Experiments were performed on two coils of a type found in commercial 10 kV motors, with artificially created defects designed to be similar to commonly occurring practical defects. Two water pumps in a nuclear plant were also selected for the investigation. Results are then analyzed and discussed.

2. Theory and Modeling

2.1. Coils for the Experiment

The structure of the stator winding coil rated at 6.6 kV is shown in Figure 2. There are six turns in total, and each turn consists of two copper strands. The overall length consists of two sections, the straight and end-winding section. For half of the coil, the straight section (wrapped by ECP and SCP) has a length of 1.3 m. The end sections beside sum to 1.1 m. The total coil length is 28.8 m, and the straight section length is 15.6 m.

Preprints (www.preprints.org) | NOT PEER-REVIEWED | Posted: 9 August 2023 doi:10.20944/preprints202308.0754.v1

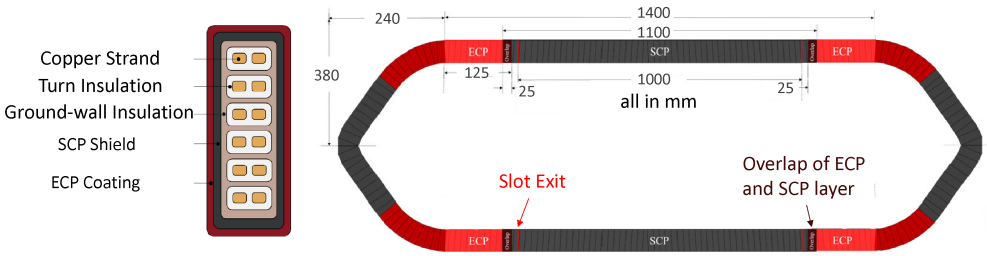

Figure 2. Structure and dimension overview of the stator coil under investigation.

Most of the straight section is placed in the stator core slot; this part is wrapped with a semi-conductive tape for slot corona protection (SCP). Beyond this, a stress-grading coating known as end corona protection (ECP) based on the nonlinear conduction of silicon carbide grains, is wrapped around the slot exit area. ECP reduces the local surface stress to prevent surface discharge around the slot exit area. The conductivity is negligible when the applied voltage is low but increases dramatically when voltage approaches the nominal [15]. It sometimes has a dominating influence on the overall dielectric response, which makes the routine testing results difficult to interpret [16].

2.2. Frequency Domain Reflectometry

The FDR is a nondestructive testing technique used to identify the change of characteristics along the length of the test object. The instrument injects a series of sinusoidal voltage signals in a broad frequency range into the test object. The scattering parameter S_{11} is the measurement result, which is defined as the ratio of the voltage leaving the port and the voltage entering the port. Then the data in frequency domain is transformed into the time domain to form a TDR-like display. The transformation algorithm is named chirp-Z Fast Fourier Transform [17], which can be automatically performed by some commercial vector network analyzers (VNA's). The TDR-like display provides a more intuitive presentation of discontinuities in the test object. The distance is calculated by multiplying the time (x-axis after transformation) with wave propagation speed.

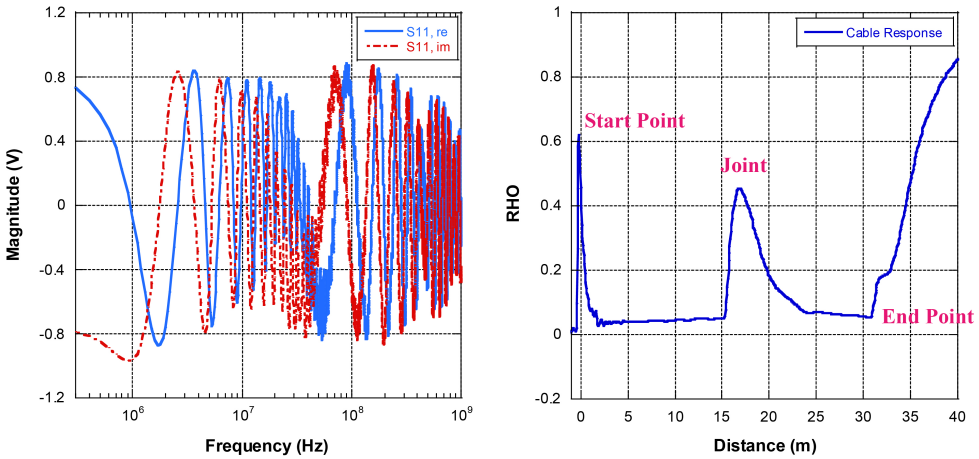

Figure 3. Illustration of the reflection signal: (**a**) frequency domain: measured scattering parameter, (**b**) time domain: transformed data.

Compared with TDR, the FDR technique has three major advantages. Firstly, the sweep frequency approach significantly increases the output energy, thus reducing the impact of propagation attenuation. Secondly, the measurement circuit with band-pass filters improves the signal-to-noise ratio [18] to achieve a much higher dynamic range. Thirdly, the spatial resolution of FDR can be as accurate as

Preprints (www.preprints.org) | NOT PEER-REVIEWED | Posted: 9 August 2023 doi:10.20944/preprints202308.0754.v1

10 cm if 1 GHz bandwidth is used [19]. These advantages give FDR sufficient sensitivity in detecting subtle condition changes so that defect characteristics can be presented more clearly.

2.3. Transmission Line Model

In the RF frequency range, the wavelength of the injected signal is comparable with or shorter than the physical size of the test object. Thus, the transmission line model with distributed circuit elements has to be used for results analysis. The model of the winding coil is shown in Figure 4. Each section of four elements ΔR, ΔL, ΔC, and ΔG represents an infinitesimally short length of the coil, which is then cascaded to model the overall behavior. The circuit elements of the slot section and end-winding section are different. The wave propagates between the coil conductor and shield (or core) in the slot section, and between the coil conductor and ground plane (or machine housing) in the end-winding section. This leads to periodic changes of distributed inductance and capacitance along the coil.

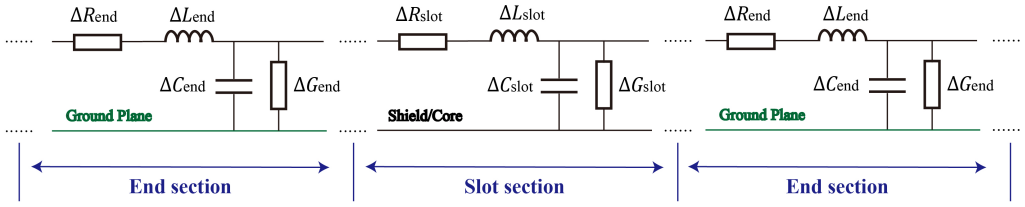

Figure 4. Equivalent circuit of the transmission line model distributed over an infinitesimally short length.

For the slot section that has a similar structure to the coaxial line, the per-unit length inductance and capacitance are written as [20]:

$$\Delta L_{slot} = \frac{\mu_1}{2\pi} \ln \frac{b}{a} \tag{1}$$

$$\Delta C_{slot} = 2\pi\varepsilon_1^{'} \ln \frac{b}{a} \tag{2}$$

where a is the inner conductor radius, b is the outer insulation radius, $\varepsilon_1^{'}$ is the permittivity of the mica paper, μ_1 is the permeability of the stator core. Although μ_1 has a much higher value than air at power frequency, it decays fast after the frequency goes above 1 kHz [21].

The end-winding section is unshielded and placed above ground during the experiment. The setup is similar to an overhead line, so the per-unit length inductance and capacitance can be approximated as:

$$\Delta L_{end} = \frac{\mu_0}{2\pi} \cosh^{-1}(\frac{h}{a}) \tag{3}$$

$$\Delta C_{end} = \frac{2\pi\varepsilon_2^{'}}{\cosh^{-1}(\frac{h}{a})} \tag{4}$$

where μ_0 is vacuum permeability, h is the height of the conductor to the ground plane, and $\varepsilon_2^{'} \approx \varepsilon_0$ is the average permittivity of the mica paper and air mixture.

If neglecting the insulation loss (ΔG), the characteristic impedance of the motor coil can be written as:

$$Z_1 = \sqrt{\frac{L_{slot}}{C_{slot}}} \tag{5}$$

$$Z_2 = \sqrt{\frac{L_{end}}{C_{end}}} \tag{6}$$

Preprints (www.preprints.org) | NOT PEER-REVIEWED | Posted: 9 August 2023 doi:10.20944/preprints202308.0754.v1

The wave propagation speed is given by:

$$v_1 = \frac{1}{\sqrt{L_{slot}C_{slot}}} \tag{7}$$

$$v_2 = \frac{1}{\sqrt{L_{end}C_{end}}} \tag{8}$$

The wave propagation speed in dielectrics is proportional to $1/\sqrt{\varepsilon_r'}$ of the light speed in free-space. The propagation speed in unshielded objects with mainly air in the surroundings is close to the free-space light speed [22].

The x-axis format obtained after transforming the frequency domain data is time. Multiplying the time with half of the propagation speed changes the x-axis to distance. The relationship between the y-axis data and wave impedance can be expressed by Equation (9). The reflection is equal to $+1$ when the test terminal is open (infinite impedance), -1 when the test terminal is short (zero impedance), and 0 if the test object impedance perfectly matches with the instrument and its test leads (50Ω).

$$RHO(x) = \frac{Z_{eq}(x) - 50\Omega}{Z_{eq}(x) + 50\Omega} \tag{9}$$

There are three typical ways to present the FDR results. The first way is named step response, which is expressed by Equation (9). It represents the wave impedance that is determined by the local mechanical and insulation property. The second way is the impulse response, which is identical to the traditional TDR trace. Mathematically it is equal to the derivative of the step response, which indicates the spot where wave impedance change happens. The third way is the impulse response in logarithmic scale, which can better present the reflection characteristic with a small magnitude.

2.4. Experimental Setups

The instrument used for stator winding FDR measurements is the commercial CHAR system. It is integrated with a high-performance VNA and automatically performs transformation after the scattering parameter S_{11} is obtained. The experiment setup of stator winding coils is shown in Figure 5. The straight portion of the coils was wrapped with the conductive copper tape acting as the stator core/ground.

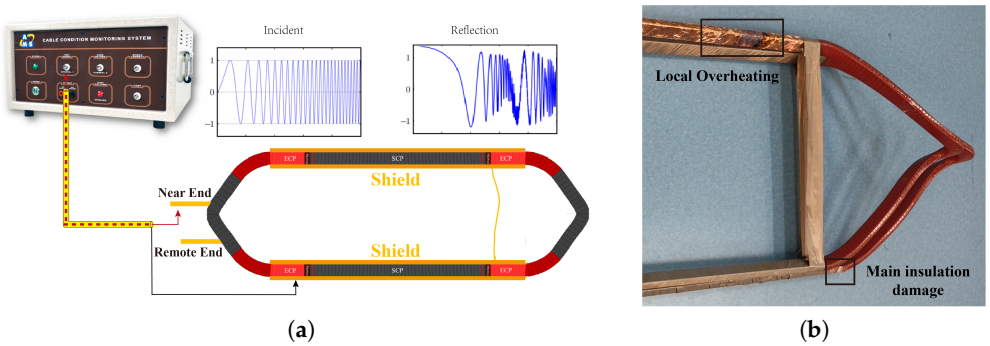

(**a**) (**b**)

Figure 5. FDR measurement setup for the stator coils: (**a**) Structure and dimension overview, (**b**) artificial faults made to the coils.

Five typical faults that are commonly seen in practice [23] were artificially made to the coils:

- End-winding discharge caused by main insulation damage, physically located at 2.25 m from the test terminal (near end);
- Tracking between coils at the winding-end section;

Preprints (www.preprints.org) | NOT PEER-REVIEWED | Posted: 9 August 2023 doi:10.20944/preprints202308.0754.v1

- Turn-to-turn short between the first and second turn, physically located at 2.4 m from the test terminal;
- Loose coil, simulated by loosening copper shield by 20 cm;
- Local overheating;

A low resistive path from the conductor to the shield was created for the end-winding discharge and tracking between coils faults. For the shorted turn-to-turn fault, two adjacent coil turns were connected by a thin wire.

In addition to the lab experiment, two sister water pumps in a nuclear power plant were also tested during shut-down maintenance. These pumps were manufactured in 2002 and are rated at 250 kW. They are definitely aged but passed all routine testings. The connection diagram for the pumps is shown in Figure 6. Three phases were measured and compared.

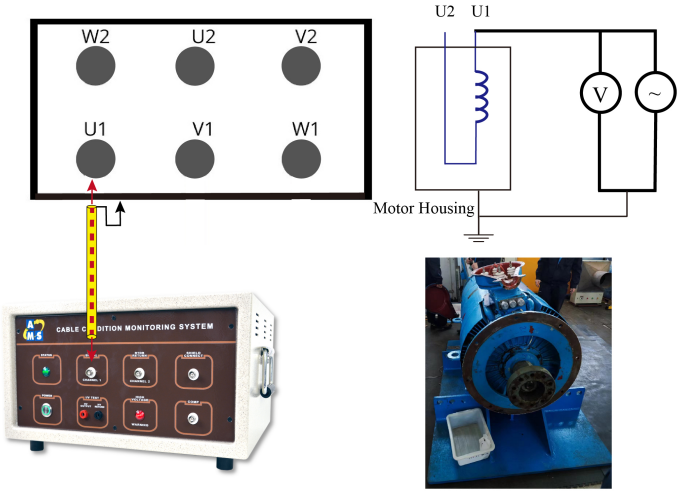

Figure 6. Schematic diagram of motor FDR testing in the field.

3. Results

3.1. FDR results of Good Coils

The coil in good condition was measured by the CHAR system as the first step. The voltage is injected at the near end terminal, with the remote end open and shorted to ground (shield), respectively. The time-magnitude results were obtained by transforming the scattering parameter S_{11} into time domain. Results are shown as step response in Figure 7, impulse response (similar to traditional TDR) in Figure 8. The FDR results with the remote end open and shorted start to diverge after 161 ns, which indicates the coil end. The deviation can be observed clearly from the traces of the step response and impulse response with y-axis in the logarithm scale. The impulse response with y-axis in linear scale needs to be zoomed in a lot before differences can be observed. Consequently, the step response and impulse response in the logarithm scale are selected for results presentation.

Preprints (www.preprints.org) | NOT PEER-REVIEWED | Posted: 9 August 2023 doi:10.20944/preprints202308.0754.v1

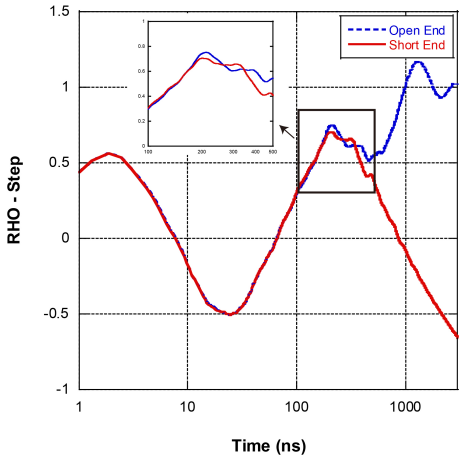

Figure 7. Step response of the coil in good condition - blue trace: remote end open, red trace: remote end short.

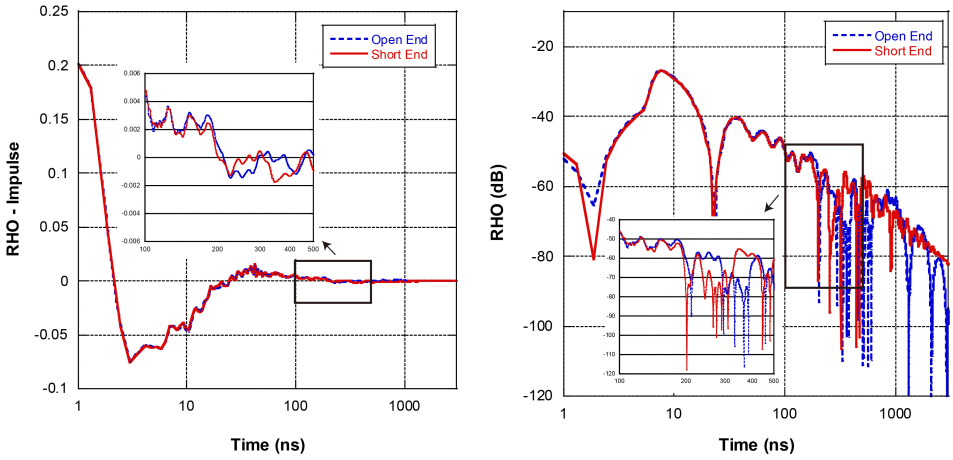

(**a**) (**b**)

Figure 8. Impulse response of the coil in good condition: (**a**) y-axis in linear scale, (**b**) y-axis in logarithm scale.

Given the designed coil conductor length of 28.8 m, the reflection at 161 ns indicates that the wave propagates with an average speed of 179 m/µs. If the propagation speed in the unshielded section is assumed to be equal to the free-space light speed, then the propagation speed in the shielded section would be 133 m/µs. This implies that the relative permittivity of the epoxy-mica insulation ε_r' is around 5, which is a reasonable value. Multiplying the time when reflection is received with 179 m/µs gives the distance from the test terminal, which represents the fault location.

The frequency band has an important effect on measurement results [24]. The ideal transformation to the time domain requires frequency domain data in the range of DC to $+\infty$. Figure 9 shows the time-transformed results using four frequency bands. The frequency band with a higher upper-frequency limit improves spatial resolution. It helps identify minor discontinuity, but the reflected voltage attenuates more. The 9 kHz - 450 MHz frequency band seems a good compromise between spatial resolution and attenuation.

Preprints (www.preprints.org) | NOT PEER-REVIEWED | Posted: 9 August 2023 doi:10.20944/preprints202308.0754.v1

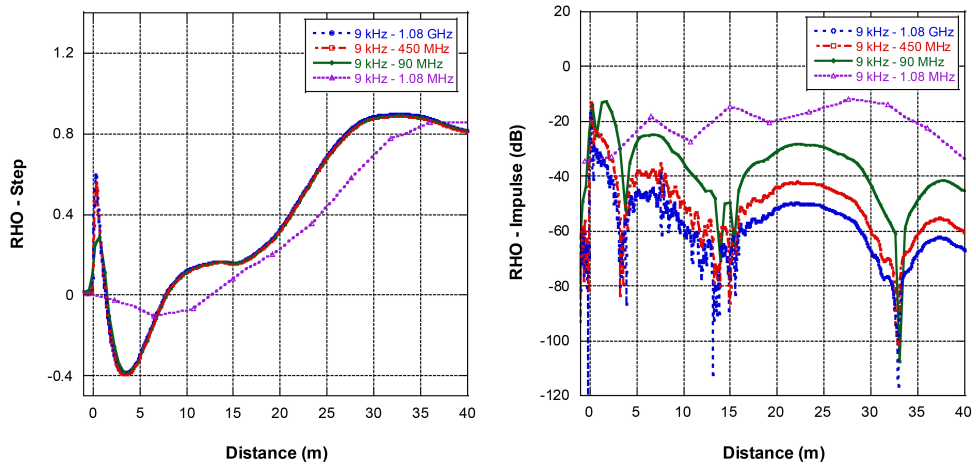

(**a**) (**b**)

Figure 9. Impact of the test frequency band on the FDR results (the x-axis is changed to distance by multiplying the propagation speed): (**a**) step response, (**b**) impulse response in logarithm scale.

3.2. Coil Fault Study

End-winding discharge can happen due to ECP degradation, insulation aging, or contamination. A low resistive path from the coil conductor to shield was created at the location about 2.25 m from the near end. FDR measurements were performed at the near and remote end, respectively. Results in Figure 10 show that the corresponding fault locations are 2.6 m and 2.2 m. Both the step and impulse response give clear fault indications. The characteristic is more prominent when the measurement is performed at the terminal close to the fault.

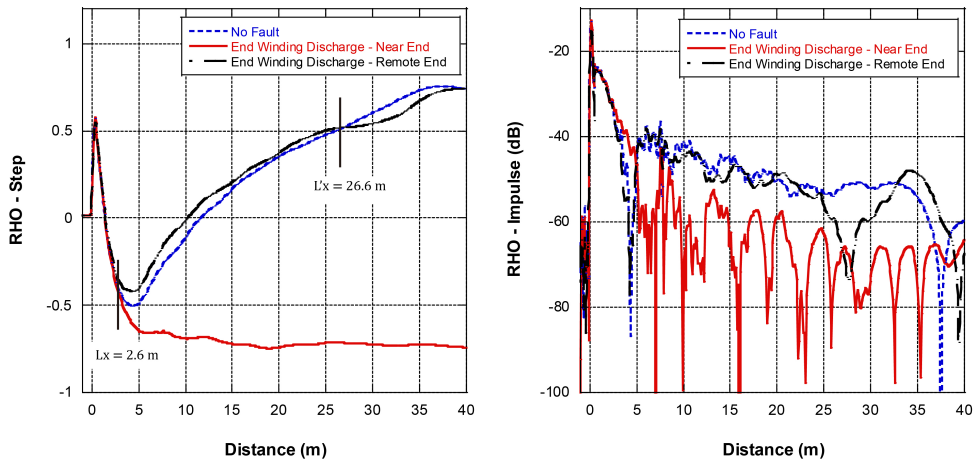

(**a**) (**b**)

Figure 10. FDR results of the coil with the end winding discharge fault: (**a**) step response, (**b**) impulse response in logarithm scale.

Stresses due to transient overvoltage in the supply is a factor that contributes to turn-to-turn short failure over time [25]. Two coil turns were shorted, and the corresponding FDR results were shown in Figure 11. Both the step and impulse response is sensitive to the turn-to-turn short failure. The step response drops starting from the fault location, and the apparent coil length is reduced.

Preprints (www.preprints.org) | NOT PEER-REVIEWED | Posted: 9 August 2023 doi:10.20944/preprints202308.0754.v1

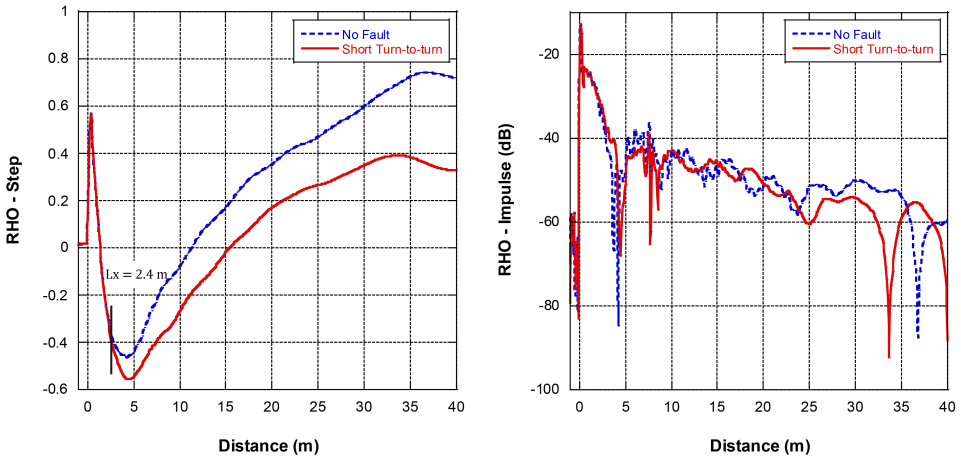

Figure 11. FDR results of the coil with the end winding discharge fault: (**a**) step response, (**b**) impulse response in logarithm scale.

Loose slot-wedge and SCP coating abrasion can happen due to machine vibration. In such a fault condition, the distributed capacitance of the slot section changes accordingly. The fault increases the step response starting from the fault location, and the apparent coil length is reduced.

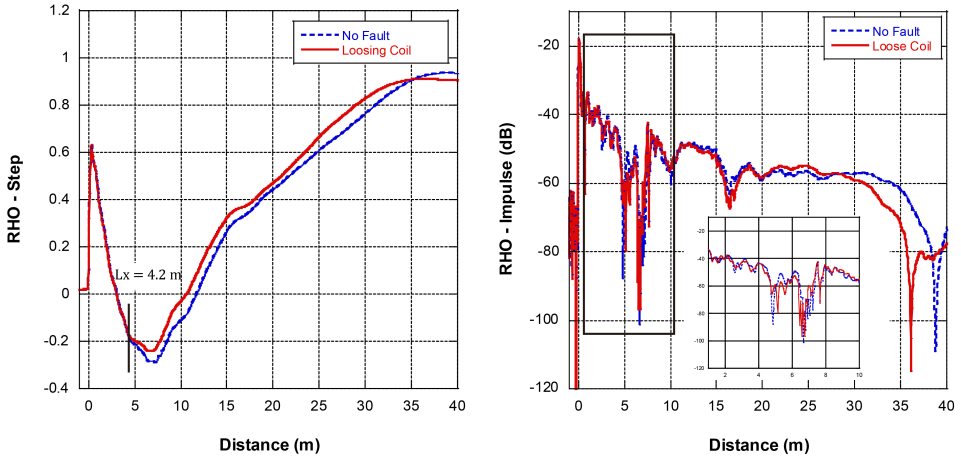

Figure 12. FDR results of the coil with the loose slot-wedge defect: (**a**) step response, (**b**) impulse response in logarithm scale.

Local overheating thermally stresses the winding insulation, contributing to main insulation delamination. A small segment in the slot section of the coil was heated by a flame, then FDR measurement was performed. Even though the IR results changed from 187.3 GΩ to 127.8 GΩ, both readings indicate good condition. For the FDR results, the change of step response due to local overheating is negligible. A periodic oscillation pattern is observed from the impulse response trace. This is because all of the six turns have the locally overheated spot. The apparent coil length remains constant.

Preprints (www.preprints.org) | NOT PEER-REVIEWED | Posted: 9 August 2023 doi:10.20944/preprints202308.0754.v1

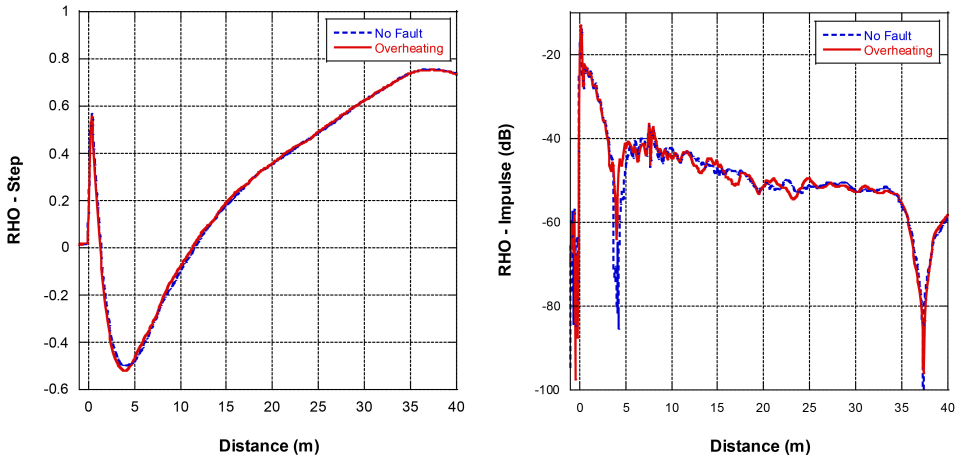

(**a**) (**b**)

Figure 13. FDR results of the coil with the local overheating defect: (**a**) step response, (**b**) impulse response in logarithm scale.

Tracking between coils can happen due to insufficient spacing between end windings and/or contamination. In the experiment, two coils were connected in series, and a low-resistive path was created between two winding-end sections. The fault changes both the step and impulse response starting from the tracking spot.

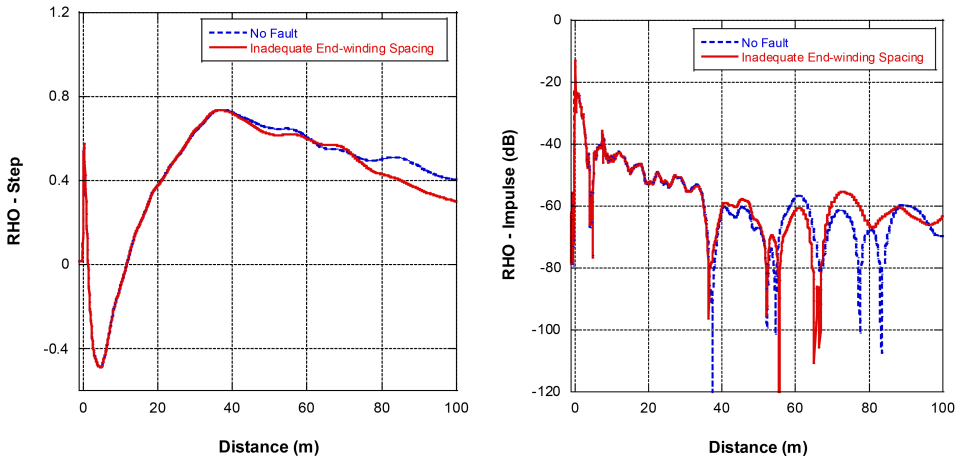

(**a**) (**b**)

Figure 14. FDR results of the tracking between two coil winding-end section fault: (**a**) step response, (**b**) impulse response in logarithm scale.

3.3. Field Application

Two water pumps were removed from service for maintenance. They had been operating in high humidity, high temperature, and corrosive environment for around 20 years. FDR measurements were performed on the three phases separately, with other phases floating and with the non-measured end of the measured phase open. Results are shown in Figures 15 and 16. The total conductor length of each phase is about 30 m. One more reflection peak was observed from the pump results compared to the coil experiment in the lab. This could be due to the winding inductance increase with the existence of a real core.

Despite the long service period of these pumps, good agreement of three-phase step responses is observed. This supports the decision that these pumps can be back in service. The connector-like reflections exist at locations of 18 m for Phase B of Motor #1, and 9 m for Phase C of Motor #2. Trending will be helpful for decision-making after successive measurements are performed.

Preprints (www.preprints.org) | NOT PEER-REVIEWED | Posted: 9 August 2023 doi:10.20944/preprints202308.0754.v1

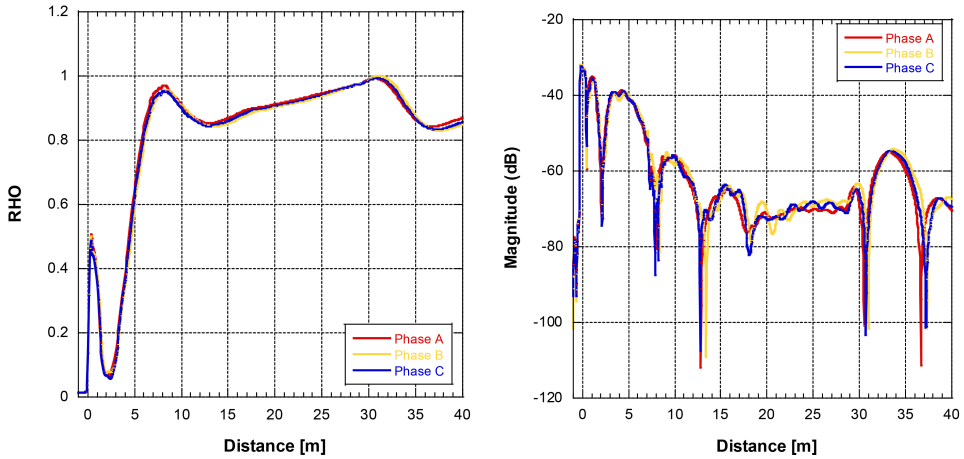

(**a**) (**b**)

Figure 15. Three-phase FDR results of pump #1: (**a**) step response, (**b**) impulse response in logarithm scale.

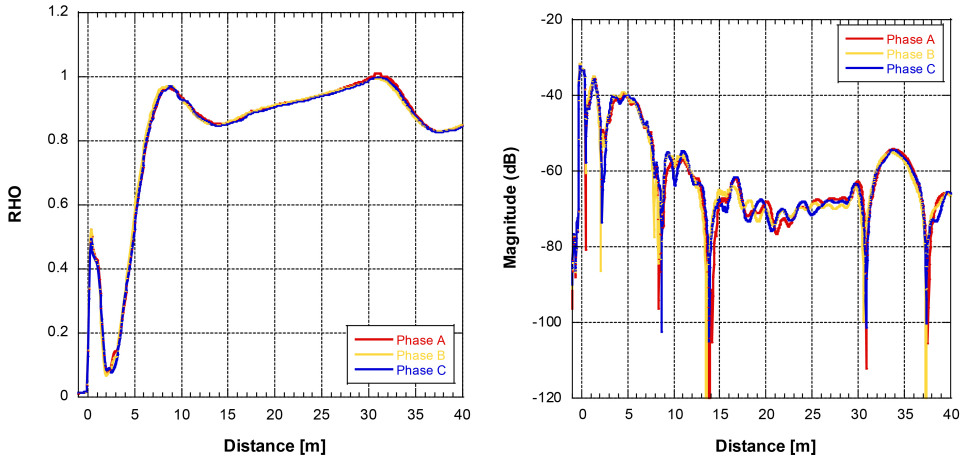

(**a**) (**b**)

Figure 16. Three-phase FDR results of pump #2: (**a**) step response, (**b**) impulse response in logarithm scale.

4. Discussion

Compared with cables, rotating machines have a more complex design in terms of structure and material. The post-curing process and the nonlinear stress grading material often make the results interpretation difficult. As stator windings are cured together with the core in the manufacturing process, faults in the slot section are hard to be verified by visual inspection. The FDR technique is specialized in location degradations by indicating the wave impedance discontinuities along the measured winding, which might have the potential to mitigate these problems.

TDR and IR testings were also performed during the experiment. TDR did not provide meaningful results due to insufficient spatial resolution. IR testing detected the low resistance fault between the conductor and shield very well. But it could not identify the shorted turn-to-turn fault. The loose coil fault and local overheating changed the resistance readings. But the values were higher than 10 GΩ in both healthy and fault conditions, which would be regarded as normal for field applications.

The interpretation of FDR results is based on the magnitude change and apparent winding length. All faults except local overheating reduce the apparent winding length. It is advisable to perform the test on both terminals, as the characteristic is more prominent if the test terminal is closer to the fault. Two measurements with the other terminal open and shorted to the ground is recommended if the propagation speed is unknown. Extensive field testing results of cables, and the experiment conducted

 doi:10.20944/preprints202308.0754.v1

in this project, suggest that the change of local inductance and/or capacitance causes a reflection most of the time. But in cases of high resistance defects, concluding the fault type and its severity is not easy, especially when several reflections are presented along the object length. As a result, the FDR result interpretation needs expertise, and more research work is needed.

5. Conclusions

This paper investigates whether the FDR technique can be used for high voltage rotating machine condition diagnosis. The FDR testing performs a broadband frequency sweep, measures the scattering parameter S_{11}, and then transforms the data into the time domain. The approach improves the measurement sensitivity and spatial resolution. This technique has been well-accepted in the nuclear power industry for cable condition diagnosis and fault locating, both shielded and unshielded types. Two motor coils with artificially-made defects commonly seen in practice and two water pumps in the field were selected as the test objects for the study. The interpretation of the FDR results was achieved by comparison, with the baseline for the coils and between three phases for the pumps. The outcome shows that FDR has sufficient sensitivity in detecting and locating those local defects in the coil. No noticeable deviations between three phases, and good routine testing results supported the decision that pumps could be put back into service. According to [14], global aging evaluation is the weakness of FDR as no reflections will be introduced. Even though further investigations are required to validate its effectiveness, adopting FDR as a complement to routine testings would be beneficial.

Author Contributions: Jialu Cheng initiated this research project and coordinated all activities. Jialu Cheng, Yizhou Zhang, Hao Yun, and Liang Wang planned and performed the lab work and field measurements together. Nathaniel Taylor provided tutorials on the modeling approach and helped with the result analysis.

Data Availability Statement: The datasets used in this paper can be downloaded via https://pan.baidu.com/s/197-sd7jMcH0_a0rp8rjTdQ?pwd=coa9.

Acknowledgments: The authors gratefully acknowledge Björn Holmgren from ABB Motors for designing and making the motor coils for the experiment, Darrell Mitchell and Casey Sexton from AMS corporation for providing the CHAR system and invaluable tutorials on the FDR subject.

Conflicts of Interest: The authors declare no conflict of interest.

References

1. Thorsen, O. V.; Dalva, M. Failure identification and analysis for high voltage induction motors in petrochemical industry. In Proceedings of the 1998 IEEE Industry Applications Conference, Thirty-Third IAS Annual Meeting, St. Louis, MO, USA, 1998; pp. 291–298.
2. Ertugrul, N.; Soong W.; Dostal G.; Saxon D. Fault tolerant motor drive system with redundancy for critical applications. In Proceedings of the IEEE 33rd Annual IEEE Power Electronics Specialists Conference, Cairns, QLD, Australia, 2002; pp. 1457–1462.
3. Rodriguez, P.; Sahoo, S.; Pinto, C.; Sutowicz, M. Field Current Signature Analysis for Fault Detection in Synchronous Motors. In Proceedings of the IEEE 10th International Symposium on Diagnostics for Electrical Machines, Power Electronics and Drives (SDEMPED), Guarda, Portugal, 2015; pp. 246–252.
4. Tallam, R.M.; Lee, S.B.; Stone, C.G.; Kliman, G.B.; Yoo, J.; Habetler, T.G.; Harley, R.G. A survey of methods for detection of stator related faults in induction machines. In Proceedings of the IEEE International Symposium on Diagnostics for Electric Machines, Power Electronics and Drives(SDEMPED), Atlanta, GA,USA, 2003; pp. 35–46.
5. Farahani, M.; Borsi, H.; Gockenbach, E. Dielectric response studies on insulating system of high voltage rotating machines. *IEEE Transactions on Dielectrics and Electrical Insulation* **2006**, *13*, pp. 212–226.
6. David, E.; Lamarre, L. Progress in DC Testing of Generator Stator Windings: Theoretical Considerations and Laboratory Tests. *IEEE Transactions on Energy Conversion* **2010**, *25*, pp. 49–58.
7. IEEE 62.2-2004 *IEEE Guide for Diagnostic Field Testing of Electric Power Apparatus - Electrical Machinery*; IEEE Standard, 2004.

8. Farahani, M.; Borsi, H.; Gockenbach, E.; Kaufhold, M. Partial discharge and dissipation factor behavior of model insulating systems for high voltage rotating machines under different stresses. *IEEE Electrical Insulation Magazine* **2005**, *21*, pp. 5–19.
9. Zhang, Y.; Yun, H.; Cheng, J.; Taylor, N. An Intelligent and Automated Online System for Condition Monitoring of Mission-Critical Induction Motors. In Proceedings of the International Council on Electrical Engineering Conference (ICEE), Seoul, Korea, 2022; pp. 934–939.
10. Renforth, L.; Giussani, R.; Knutsen, T.; Aardal, B.; Kienner, T.E. A novel solution for the reliable online partial discharge monitoring (olpd) of vsd-operated EX/ATEX HV motors. In Proceedings of the 2016 Petroleum and Chemical Industry Conference Europe (PCIC Europe), Berlin, Germany, 2016; pp. 1–9.
11. Cusido, J.; Romeral, L.; Ortega, J.A.; Rosero, J.A.; Garcia, E.A. Fault Detection in Induction Machines Using Power Spectral Density in Wavelet Decomposition. *IEEE Transactions on Industrial Electronics* **2008**, *55*, pp. 633–643.
12. IEC 60076-18:2012 *Power transformers - Part 18: Measurement of frequency response*, 1st ed.; International Standard, 2012.
13. Fantoni, P.F. *NPP wire system aging assessment and condition monitoring state-of-the-art report*; Institutt for energiteknikk, OECD Halden Reactor Project: Halden, Norway, 2004.
14. Glass, S.W.; Jones, A.M.; Fifield, L.S.; Hartman T.S. *Bulk and Distributed Electrical Cable Non-Destructive Examination Methods for Nuclear Power Plant Cable Aging Management Programs*; Pacific Northwest National Laboratory: Washington, US, 2016.
15. Roberts, A. Stress grading for high voltage motor and generator coils. *IEEE Electrical Insulation Magazine* **1995**, *11*, pp. 26–31.
16. Cheng, J.; Taylor, N.; Werelius, P. Nonlinear Dielectric Properties of the Stator and Transformer Insulation Systems. *IEEE Transactions on Dielectrics and Electrical Insulation* **2022**, *29*, pp. 240–246.
17. Oppenheim, A.V.; Schafer, R.W. *Discrete-Time Signal Processing*; Prentice Hall: Englewood Cliffs, New Jersey, England, 1989.
18. Keysight Technologies Application Note: Time Domain Analysis Using a Network Analyzer. Available Online: https://www.keysight.com/us/en/assets/7018-01451/application-notes/5989-5723.pdf (accessed on 31 July, 2023).
19. MOHR Test and Measurement LLC Application Note: TDR vs. FDR: Distance to Fault. Available Online: https://www.mohr-engineering.com/TDR_vs_FDR_Distance_to_Fault-A.php (accessed on 31 July, 2023).
20. Pozar, M.D. *Microwave Engineering*, 3rd ed.; Wiley: Hoboken, New Jersey, US, 2012; pp. 49–64.
21. Abeywickrama, N.; Serdyuk, Y.; Gubanski, S. High-Frequency Modeling of Power Transformers for Use In Frequency Response Analysis. *IEEE Transactions on Power Delivery* **2008**, *23*, pp. 2042–2049.
22. Alam, M.N.; Coats, D.; Dougal R.A.; Ali, M. Surface wave propagation measurements in unshielded XLPE power cables. In Proceedings of the IEEE Antennas and Propagation Society International Symposium (APSURSI), Orlando, FL, USA, 2013; pp. 1770–1771.
23. Stone, C.G. *Electrical Insulation For Rotating Machines—Design, Evaluation, Aging, Testing and Repair*; IEEE Press: Piscataway, New Jersey, US, 2004; pp. 137–174.
24. Glass, S.W.; Fifield, L.S.; Jones, A.M.; Hartman T.S. Frequency domain reflectometry modeling and measurement for nondestructive evaluation of nuclear power plant cables. In Proceedings of the 18th International Conference on Environmental Degradation of Materials in Nuclear Power Systems – Water Reactors, Online Conference, 2017; pp. 1267–1280.
25. Kumar, S. et al. A Comprehensive Review of Condition Based Prognostic Maintenance (CBPM) for Induction Motor. *IEEE Access* **2019**, *7*, pp. 90690–90704.